Airborne magnetics as structural guide in the 3D inversion of Airborne EM data

Carsten Scholl
CGG
Address
Carsten.Scholl@CGG.com

Stephen Hallinan
CGG
Address
Stephen.Hallinan@CGG.com

Marianne Parsons
CGG
Address
Marianne.Parsons@CGG.com

Tom Kimura
CGG
Address
Tom.Kimura@CGG.com

SUMMARY

Airborne Magnetics and Electromagnetics surveys are widely used in mineral resource exploration. Beyond the sensitivity of both to certain mineral deposits, magnetics serves as a useful proxy for geological structure.

We extend our previous work on cross-gradient, structurally-guided 3D EM inversions to use two-dimensional gradients derived from pre-processed magnetic grids as a structural guide in inversions of AEM data sets

We compare 3D resistivity inversion results obtained with this structural guiding approach to those without, for AEM data recorded in a survey in New Brunswick, Canada.

This structurally-guided 3D inversion method using magnetics data is generic and can be applied to inversion of other geophysics data such as ground electromagnetics, etc.

Key words: 3D inversion, joint inversion, AEM, magnetics, structural constraint.

INTRODUCTION

The Airborne Electromagnetic (AEM) method has been widely adapted in the mining industry to detect large mineral deposits with conductive material. The data is either interpreted either using maps of simple conductivity transforms (Huang and Fraser, 1996) or resistivity models obtained by using 1D (Farquharson et al., 2003; Vallée and Smith, 2007) or – more recently – multidimensional inversion algorithms (Cox and Zhdanov, 2008; Haber and Schwarzbach, 2014, Scholl and Miorelli, 2019).

In addition to standalone magnetics surveys at regional and prospect scale surveys – a useful proxy for geological trends as well as deposit detection – magnetics data are frequently measured simultaneously with AEM surveys. Combined interpretations are usually qualitative, however.

In this paper, we present a quantitative approach to use the magnetic data directly during the AEM inversion, but as a structural guide to the 3D resistivity inversion rather than a joint inversion of the resistivity and magnetic susceptibility volumes. The goal is to derive, out of the models that sufficiently explain the data, a resistivity volume that more closely resembles structures that are visible in the magnetic anomaly maps.

For this, we employ the cross-gradient approach (Gallardo and Meju, 2003), originally intended to structurally link two properties in a joint inversion of different parameters, since extended to support certain geological structures in the inversion of a single method. This application of the method relates the gradients of the model that are inverted with the gradients defined by some structural reference. Previous examples used a known regional strike (Scholl et al., 2015), near surface dip measurements or seismic volumes (Scholl et al., 2017) or complex geological models (Mackie et al., 2020) to define these reference gradients.

In all of the 3D examples, the gradients were also 3D vectors. However, if we want to use a 2D structural map of the area in a 3D inversion, the algorithm needs some small but important changes to get to useful results. In this paper, we show the required modifications to the algorithm and demonstrate its use on a real data set.

METHOD

A linearized inversion is typically formulated in terms of a quadratic cost function that needs to be minimized. Often, the cost function contains a part that relates to the data misfit and one that relates to the roughness of a model (e.g. Constable et al., 1987):

$$\Phi(\mathbf{m}) = \|\mathbf{d} - \mathbf{f}(\mathbf{m})\|^2 + \beta \int_V \|\nabla\mathbf{m}\|^2 dV,$$

Here, Φ is the cost function, $\mathbf{m}$ is the model vector, $\mathbf{d}$ and $\mathbf{f}$ are the measured data and model response, respectively, and β is the trade-off parameter that weights the data misfit (the first term) against the model roughness (the second term). The roughness here is defined using the integral of the model gradient $\nabla\mathbf{m}$ as model regularization. All values in the equation above are assumed to be dimensionless.

The cross-gradient approach as published in previous papers adds an additional regularization term

$$\Phi(\mathbf{m}) = \|\mathbf{d} - \mathbf{f}(\mathbf{m})\|^2 +$$
$$\beta \int_V \|\nabla\mathbf{m}\|^2 dV + \gamma \int_V \|\nabla\mathbf{m} \times \nabla\mathbf{s}\|^2 dV,$$

where in the general case $\nabla\mathbf{s}$ is a 3D gradient of the structural model and γ is a different trade-off parameter that balances the cross-gradient term with the other two terms. The contribution of the cross-gradient term is zero when the cross product of the two gradients $\nabla\mathbf{m}$ and $\nabla\mathbf{s}$ is zero, which is the case when either the gradients are parallel or antiparallel, or when either of them is zero. Note that the amplitude of the gradient $\nabla\mathbf{s}$ only defines how strong the regularization is at a given cell.

The integral is numerically evaluated in a discrete form where the norm of the cross product is evaluated for each cell i of model. In components this yields

$$\|\nabla m_i \times \nabla s_i\|^2 = \left\| \begin{pmatrix} \partial_y m_i \partial_z s_i - \partial_z m_i \partial_y s_i \\ \partial_z m_i \partial_x s_i - \partial_x m_i \partial_z s_i \\ \partial_x m_i \partial_y s_i - \partial_y m_i \partial_x s_i \end{pmatrix} \right\|^2$$

$$= (\partial_y m_i \partial_z s_i - \partial_z m_i \partial_y s_i)^2 + (\partial_z m_i \partial_x s_i - \partial_x m_i \partial_z s_i)^2 + (\partial_x m_i \partial_y s_i - \partial_y m_i \partial_x s_i)^2,$$

where ∂_x, ∂_y and ∂_z denote partial derivative operators in x, y and z direction, respectively.

In this paper, we want to use a 2D map as a structural guide. This means that $\partial_z s_i$ is not defined. Furthermore, we want to apply the structure not only to the uppermost layer, but to all depths. For simplicity, we therefore assign the map to each grid level of our model. This means that $\partial_z s_i$ now is defined, but is $\equiv 0$ everywhere. With this, the expression above becomes

$$(\partial_z m_i \partial_y s_i)^2 + (\partial_z m_i \partial_x s_i)^2 + (\partial_x m_i \partial_y s_i - \partial_y m_i \partial_x s_i)^2.$$

To minimize this term for an arbitrary s_i, $\partial_z m_i$ needs to be $\equiv 0$ as well, so the regularization will suppress any vertical changes in the inverted model, which is not desirable. The solution is to only use the z-component of the cross product $(\partial_x m_i \partial_y s_i - \partial_y m_i \partial_x s_i)^2$ as the regularization, which means that the cross-gradient term provides no regularization to the vertical gradient of the model.

Using structural regularization in inversions

Inversions of geophysical data are inherently non-unique, either due to the physics involved or the presence of data uncertainties. The commonly applied "smooth model" inversion approach seeks to find the "simplest" possible solution to out of all the potential solutions that would yield a similar misfit (Constable et al., 1987).

The main reason for adding an additional structural regularization to the inversion is to bias the ambiguous parts of the solution closer to what the interpreter considers a geologically more plausible model that agrees better with some auxiliary structure. This can help to find a unified model across multiple methods or for hypothesis testing.

The inversion, however, is still supposed to fit the data, which means that the structural constraint can only have a noticeable effect in parts of the model that are less well resolved by the data. This means that the auxiliary texture should at least to some extend fit the structures required by the data. Otherwise, the inversion might converge at high misfits, or the trade-off parameter for the cross-gradient term γ has to be set to a value so small that the term has no effect on the inversion.
EM data by itself will overall provide a reasonable horizontal resolution of the resistivities in the near surface. So, adding an additional regularization of the horizontal structure is likely only going to work well in cases where the overall patterns that can be inferred from the EM data is to some extend similar to the auxiliary structure.

FIELD DATA EXAMPLE

The data set used in this paper is a subset of data recorded near Kedgwick, New Brunswick, available from the geoscience data repository of Natural Resources Canada (Kiss et al, 2000, see Figure 1). The data itself were recorded with a DIGHEMV system (Fraser, 1972; Bouvier et al., 1999). We used CGG's proprietary multidimensional inversion code Otze (Scholl and Miorelli, 2019) for the inversions.

In all cases we inverted the three co-planar channels at frequencies 867 Hz, 7,193 Hz, and 56,550 Hz. We assumed standard deviations of 5% plus 2, 5, and 10 PPM, respectively. As indicated in Figure 1, we inverted only a smaller subset of the data. All inversions started from a homogeneous half-space including the real topography of the area.
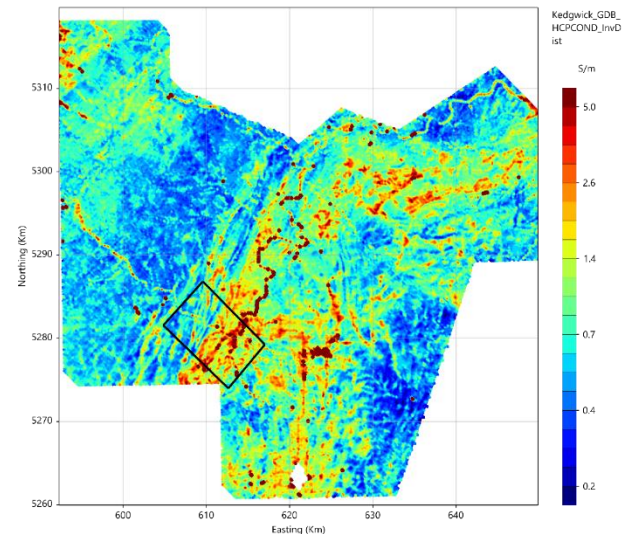
Figure 1. Map of the conductivity transform for the high frequency (56 kHz), coplanar channel of the system over the complete Kedgwick area; the black shape denotes the data mask for the inversions. Coordinates are in NAD83/UTM zone 19N.

Regular inversion of the EM data

The regular 3D smooth model inversion of the EM data reached the target misfit of a normalized root-mean-square (RMS) of 1.0 after 9 iterations. Figure 2 shows the result of the inversion at a depth of 100 m below ground level (bgl).
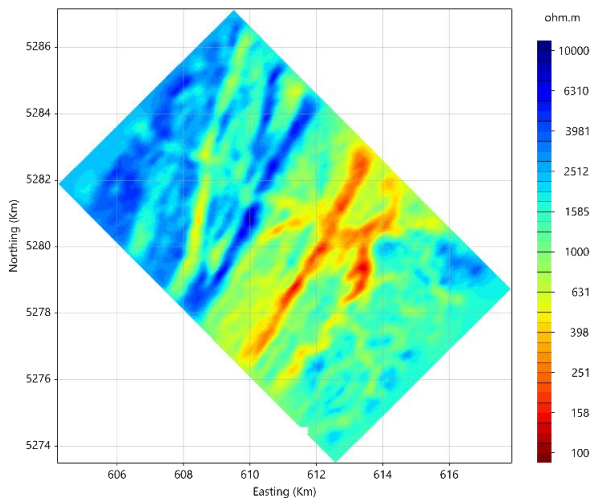
Figure 2. Inversion result for the EM data at a depth of 100 m bgl.

Magnetic data as structural constraint

Figure 3 shows the magnetic data recorded during the survey. The left subfigure shows the residual magnetic signal, that is, the measured signal minus the international geomagnetic reference field (IGRF, see Kiss, 2000). The dominant features have a relatively long wavelength. For a structural constraint, we are interested mostly in smaller scale, near surface structures. Therefore, we applied a 140m match filter to the magnetic data (Spector and Grant, 1970). The result of this filter operation is shown in the right panel of Figure 3.

For the inversion with a structural constraint, the match filtered magnetic data is mapped onto all depth levels of the 3D model domain. During the mapping, the maxima were limited to a value of 10 nT. Afterwards, the structural map was smoothed horizontally. The final structure mapped onto the model is shown in Figure 4 (left).

The inversion was started again from a homogenous half-space, including the additional regularization term for the modified cross-gradient link to the structural model. Also this inversion reached the target misfit, but it required 13 iterations. Figure 4 (right) shows the result of the inversion with the structural constraint at a depth of 100 m bgl.

For better comparison, Figure 5 shows the results of the regular inversion without structural constraint (left) and the one with the structural constraint (right). On both plots, the original, match filtered magnetic data (Figure 3, right) is superimposed with contour lines.

The inversion result with the structural constraint matches the contour lines nearly perfectly. Fundamentally, the resistivity patterns obtained from the two inversions are similar. But there are several details in which the results differ. The eastern part (red ellipse) appears less noisy on the right. Also, the hook like feature in the white ellipse is different. Without the structural constraint, the southern tip of the hook seems more connected to a linear feature that extends to the SE. The two linear features that are crossing the strike direction in the centre (black ellipse) are suppressed in the result with structural constraint.

Just because the inversion result is closer to the magnetics does not necessarily mean that it is more correct. The anomalies in

the blue ellipse are changed from a curved, linear feature (left) to individual blobs (right) as indicated in the magnetic data. It seems likely that these blobs are imprints of culture and not of geological origin.

Likewise, several of the mostly linear features (e.g. the blue one in the purple ellipse) appear with more beads along its length, because the original magnetic data exhibits these. Again, they are more likely to be artefacts of the line spacing and gridding than geologically relevant.

In order to reduce these probably artificial features we modified the filtered magnetics further manually. The figure with the filtered grid in grayscale was saved to a TIF file. It was then loaded into a picture editing tool for manual editing, using a cloning tool to remove most of the pockmarks and a smudging tool in the direction of the linear features to smooth out the beads related to the line spacing and higher frequency noise. Figure 6 shows the result of that operation on the left. The resulting TIF was then in turn mapped back onto the model (Figure 6, right).

With this structural constraint, the inversion reached the target misfit after 15 iterations, shown in Figure 7. The artificial blobs now disappeared, and the overall appearance is much smoother than both previous results while adhering well with the magnetics structural map.

Figure 8 shows a map view at 50 m bgl through the three inversion results as well as a cross section with a vertical exaggeration of three for each. "w/o structure" refers to the model that was obtained by the standard smooth model inversion, while "w/ structure" and "w/ edited structure" refer to the model with structural constraint as shown in Figure 4 and Figure 6, respectively.

The three results are overall similar, but the two that included the magnetics information look cleaner and more structurally consistent, depending of course on how geologically relevant the structural information in the magnetics is.

DISCUSSION

We derived a formulation for a cross-gradient structural constraint that is suitable for using a 2D map as structural guide in a 3D inversion. The approach was demonstrated for a field data example. The inversion result was closer to the texture of the magnetic data when the latter was used as a structural constraint, meaningful to the extent that the magnetics are a reliable guide to the geological structure.

In the first inversion example, we used magnetic data as structural constraint, and in the second case we used a manually modified "enhanced" image of the grid. At this point, the structural guide is merely generated from a georeferenced figure, so it is clear that the approach works as well with any arbitrary figure, as long as the texture is in some agreement with the measured data. For example, the user might use a geological map or a structural interpretation as the basis.

The caveat with arbitrary figures might be that those might contain structures that are finer than the cell spacing of the model, so a simple mapping as used in this paper is likely not the best approach. Instead, it would be beneficial to compute the gradients directly on the figure, use a structural tensor approach for the upscaling (Zhou et al. 2014, Scholl et al., 2017;

Kim et al., 2019) and then use these as structural constraint as shown in this paper.

ACKNOWLEDGMENTS

REFERENCES

Bouvier, A., Elkaim, P., Hodges, G., 1999, Heliborne Electromagnetic & Magnetic Surveying Applied to a Pipeline Construction Project in Canada, EEGS Annual Meeting, Budapest.

Constable, S.C., Parker, R.L., Constable C.G., 1987, Occam's inversion: A practical algorithm for generating smooth models from electromagnetic sounding data, Geophysics, 52, 289-300.

Cox, L.H., and Zhdanov, M.S., 2008, Advanced computational methods for rapid and rigorous 3D inversion of airborne electromagnetic data: Communications in Computational Physics, 3, 160–179.

Farquharson, C.G, Oldenburg, D.W., and Routh P.S., 2003, Simultaneous 1-D inversion of loop-loop electromagnetic data for magnetic susceptiblility and eletrical conductivity, Geophysics, 68, no. 6, 1857-1869.

Fraser, D.C., 1972, A new multicoil aerial electromagnetic prospecting system. Geophysics, 37, 518-537.

Gallardo, L.A., and Meju, M.A., 2003, Characterization of heterogeneous near-surface materials by joint 2D inversion of dc resistivity and seismic data. Geophys. Res. Lett., 30, 1658.

Haber, E. and Schwarzbach, C., 2014, Parallel inversion of large-scale airborne time-domain electromagnetic data with multiple OcTree meshes, Inverse Problems, 30, no. 5.

Huang, H., and Fraser, C.D., 1996, The differential parameter mapping for multifrequency airborne resisitivty mapping, Geophysics, 61, no.1, 100-109.

Kim, B., Seol, S.J., Byun, J., and Cho., S., A structure-tensor-constraint cooperative inversion using an extracted physical property distribution, Geophysical Journal International, Volume 217, Issue 2, May 2019, Pages 1334–1352, https://doi.org/10.1093/gji/ggz082.

Kiss, F., Carson, J., McCutcheon, S.R., Oneschuk, D., and Holman, P., 2000, Detailed multiparameter airborne geophysical survey data release, Kedgwick area, New Brunswick / Diffusion des données d'un levé géophysique aérien à paramètres multiples (levé détaillé), région de Kedgwick, Nouveau-Brunswick: Geological Survey of Canada, Open File 3784, 2000, 54 sheets, https://doi.org/10.4095/211491; https://open.canada.ca/en/open-government-licence-canada.

Mackie, R.L., Meju, M.A., Miorelli, F., Miller, R.V., Scholl, C., and Saleh, A.S., 2020, Seismic image-guided 3D inversion of marine CSEM and MT data. Interpretation, 8 (4) 1-13, http://dx.doi.org/10.1190/INT-2019-0266.1.

Scholl, C., Neumann J., and Watts, M.D., 2015, Geosteered 3D Inversion of Airborne EM Data in Rugged Terrain. EAGE Near Surface Geoscience (Turin) AEM Workshop Abstracts.

Scholl, C., Hallinan, S., Watts, M.D., and Mirorelli, F., 2017, Geological consistency from inversions of geophysical data: 79th EAGE Annual Meeting, Abstracts, doi: 10.3997/2214-4609.201700849.

Scholl, C., and Miorelli, F., 2019, Airborne EM inversion on vertically unstructured model grids. Exploration Geophysics, doi: 10.1080/08123985.2019.1668239.

Spector, A., and Grant, F. S., 1970, Statistical models for interpreting aeromagnetic data. Geophysics, 35, no. 2, 293-302.

Vallée, M., and Smith, R., 2007, Comparison of fixed-wing airborne electromagnetic 1D inversion methods. Proceedings of Exploration 07: 5th Decennial International Conference on Mineral Exploration, 1067–1072.

Zhou, J., Revil, A., Karaoulis, M., Hale, D., Doetsch, J., and Cuttler, S., 2014. Image-guided inversion of electrical resistivity data, Geophys. J. Int., 197, 292–309, 10.1093/gji/ggu00.
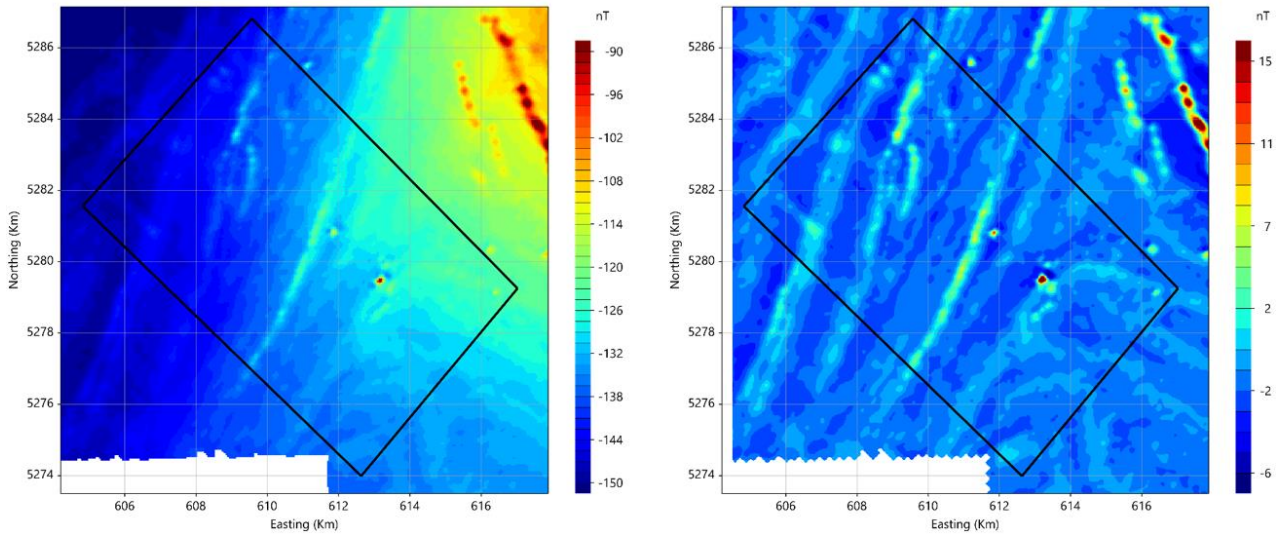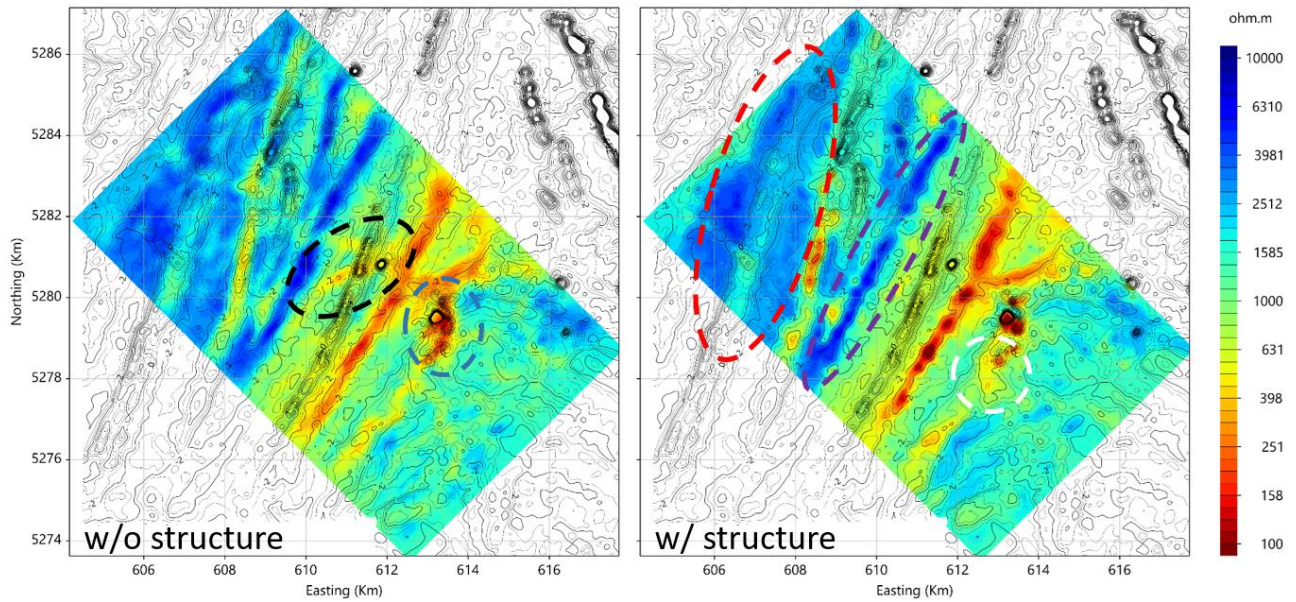
Figure 3. Magnetic data recorded in the survey; the left panel shows the total residual magnetics, the panel on the right hand the match-filtered residual used as the structural constraint in the EM inversions.
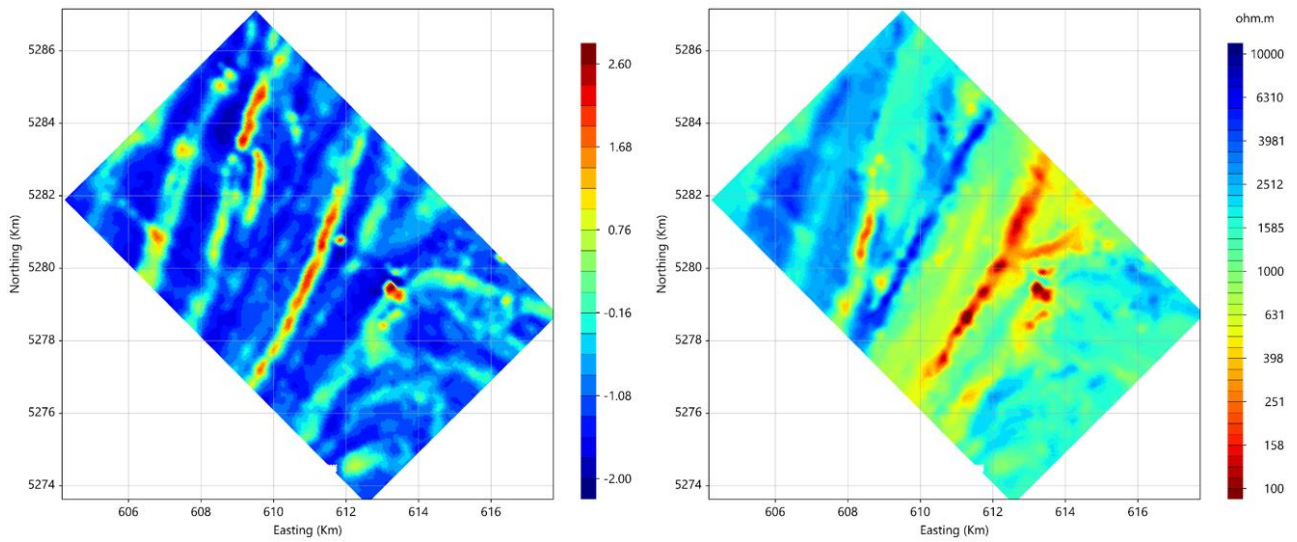
Figure 4. Filtered magnetics mapped onto the grid (left) and result of the EM inversion with structural constraint from the magnetics at a depth of 100 m bgl.
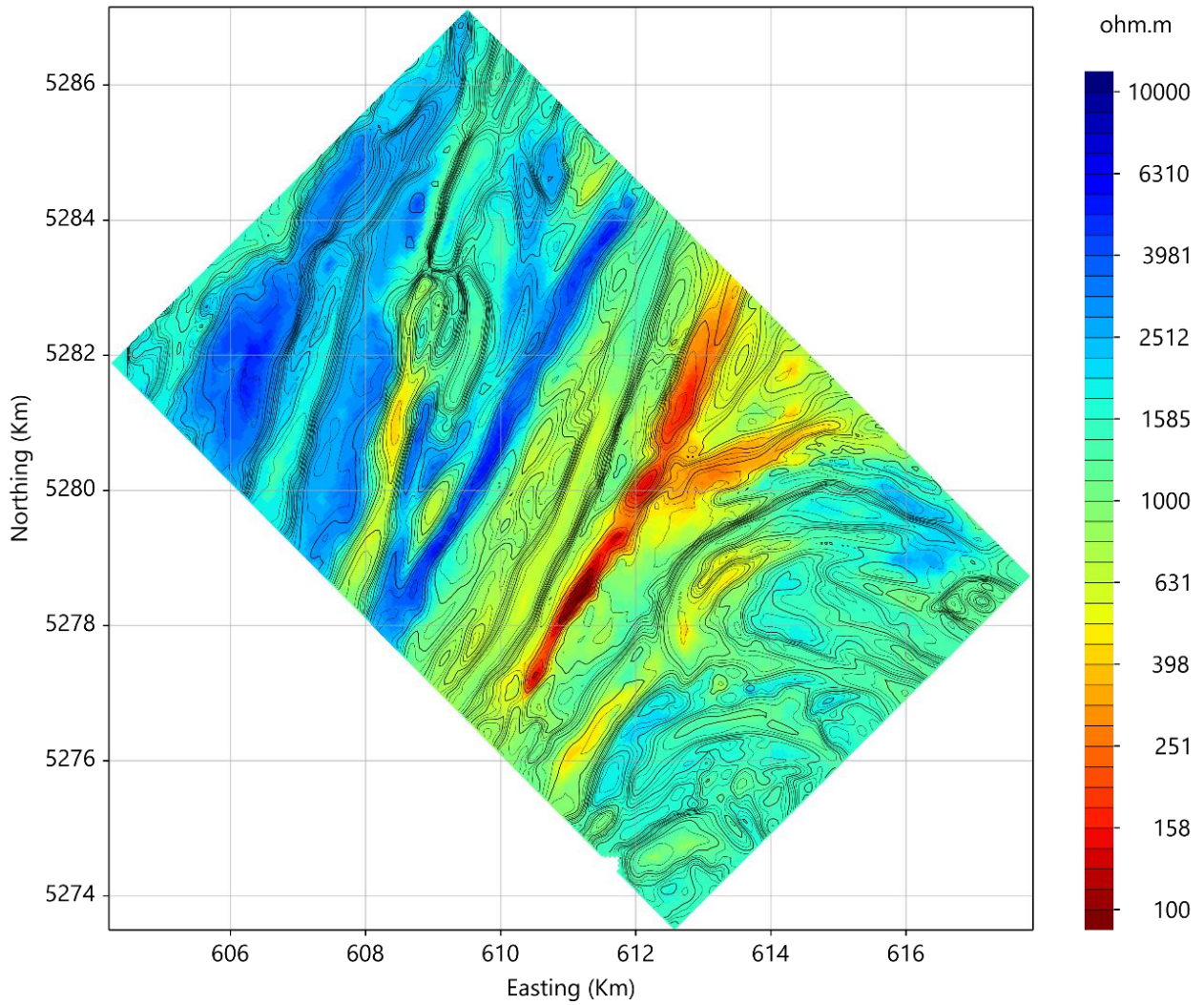
Figure 5. Results w/o (left) and w/ (right) structural constraint at 100 m bgl; superimposed as contour lines are the filtered magnetic data. The dashed ellipses mark areas discussed in the text.
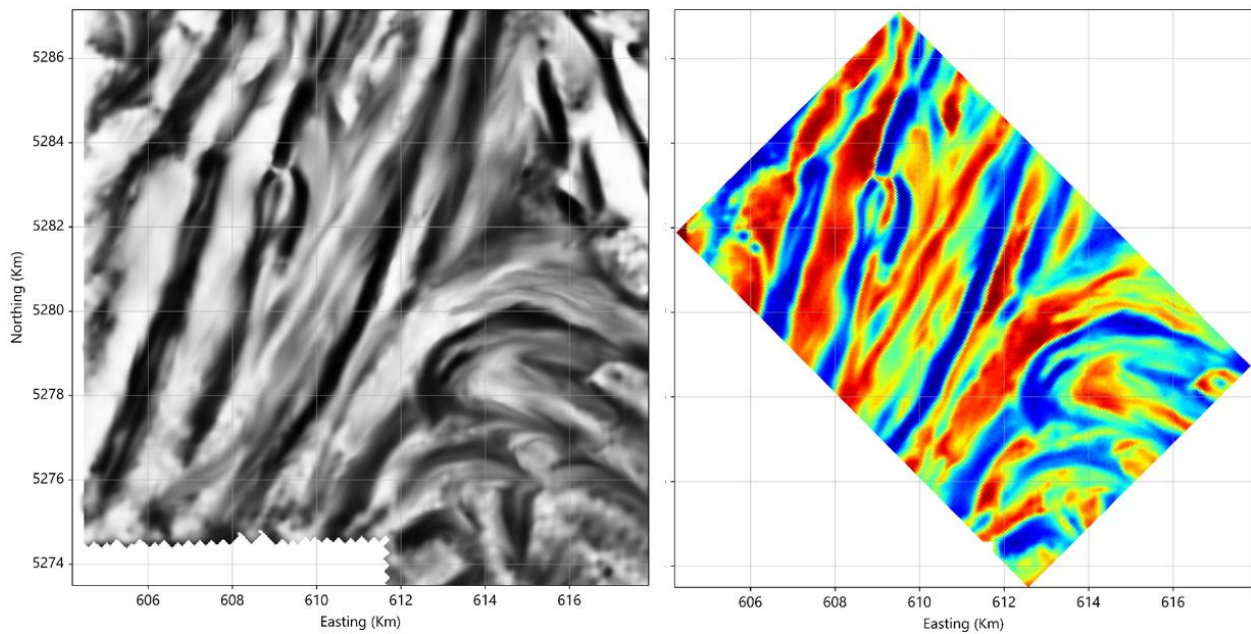
Figure 6. Modified version of the original filtered magnetics data (left) and its mapping onto the model (right).

Figure 7. Inversion result using the edited structural map from Figure 6 as structural constraint (contour lines) at a depth of 100 m bgl.
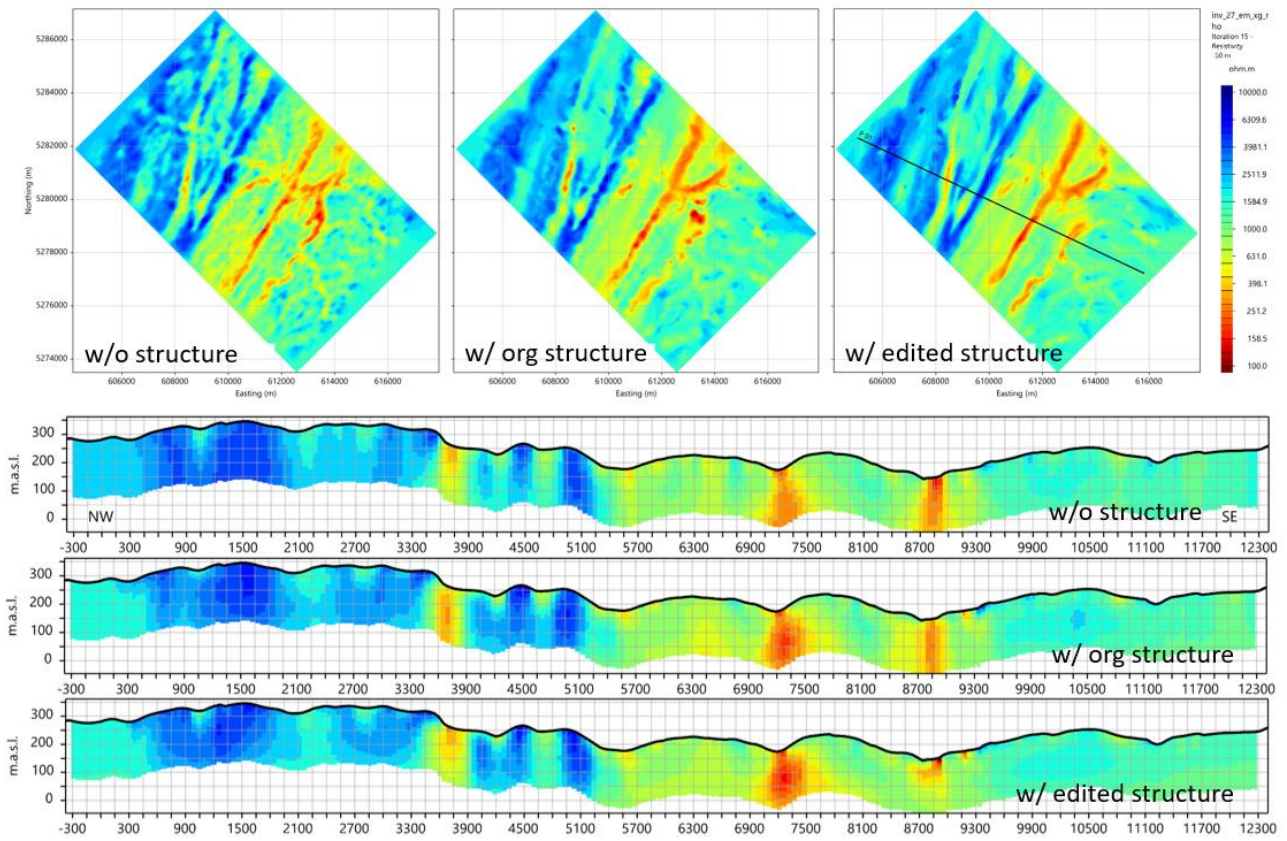
Figure 8. Comparison between the three inversion results; the top row shows the three models at a depth of 50 m bgl. The sections below are along the profile marked in the upper right map view.